Genomic variations drive phenotypic heterogeneity in pancreatic cancer cells

Gengqiang Xie[1], Olalekan H Usman[1], Sampath Kumar[1], Dhenu Patel[1], Megan Kavanaugh[1], Yue Julia Wang[1], and Jerome Irianto[1]*

[1]Department of Biomedical Sciences, College of Medicine, Florida State University, Tallahassee, FL 32306, USA

*Corresponding author: Jerome Irianto, Department of Biomedical Sciences, College of Medicine, Florida State University, 1115 West Call St, Tallahassee, FL 32306

Phone: 850-645-9438

E-mail: jerome.irianto@med.fsu.edu

Abstract

Genomic heterogeneity in pancreatic cancer has been widely studied in recent years because of the development of next generation of genome-wide sequencing technology. However, little is known whether this genomic heterogeneity will drive phenotypic heterogeneity and the underlying mechanism that links genomic variations to phenotypic heterogeneity in pancreatic cancer. To study these questions, by using single-cell flow sorting, we established four clones from MiaPaCa-2, a cell line derived from human pancreatic primary tumors. Indeed, these four MiaPaCa-2 clones show heterogenous phenotypes including distinct cellular morphology and differential proliferation and migration rate. Further genomic DNA sequencing analysis of MiaPaCa-2 clones demonstrates genomic heterogeneity, suggesting heterogeneity of the population or genomic instability. Lastly, our mRNA-sequencing analysis of the four MiaPaCa-2 clones identified that ITGAV is necessary and sufficient for morphology change of MiaPaCa-2 subclones, suggesting that ITGAV might be a major regulator in controlling the heterogeneity in MiaPaCa-2 cell line. In conclusion, our study demonstrated the heterogeneity of pancreatic cancer cells at genomic, transcriptomic, and phenotypic levels.

Key words: MiaPaCa-2, pancreatic cancer, heterogeneity, ITGAV

Introduction

Pancreatic ductal adenocarcinoma (PDAC) is one of the most lethal types of cancer with a 5-year survival rate of 7%, mainly due to lack of diagnosis at an early stage and its strong chemoresistance (*1, 2*). PDAC tumor heterogeneity is evident at the histological level, both between tumors and within a tumor. Recent high-throughput analyses have confirmed pancreatic cancer heterogeneity at the genomic, transcriptomic, and metabolomic level (*3-10*). However, very few studies focus on the phenotypic and genomic heterogeneity at the cellular level. Additionally, it's still mysterious how the genomic and transcriptomic heterogeneity translates to the phenotypic heterogeneity in PDAC.

In this study, we used MiaPaCa-2, one of the most commonly used tumor cell lines for *in vitro* studies of PDAC carcinogenesis (*11, 12*). First, we isolated and established four MiaPaCa-2 clones by single cell flow cytometry that display clear morphological differences. Further studies found that the MiaPaCa-2 clones show phenotypical heterogeneity including distinct cell proliferation and migration rate. Then, using single-nucleotide polymorphism microarray, we observed genomic heterogeneity in the form of chromosome copy number alterations within the MiaPaCa-2 clones. By using the transcriptomic analysis, we identified a gene encoded *Integrin Subunit Alpha V* (*ITGAV*) that is required for morphological heterogeneity of MiaPaCa-2 cells. In summary, our study systematically investigated the heterogeneity of PDAC cells at the phenotypic, genomic, and transcriptional levels and found how the genomic and transcriptional heterogeneity impacts phenotypic heterogeneity in MiaPaCa-2 PDAC cells.

Results

Morphological heterogeneity of MiaPaCa-2 clones

To study whether heterogeneity exists in pancreatic cancer cells, we first flow sorted a single cell into each well of a 96-well plate from the pancreatic cell line, MiaPaCa-2 by forward scatter flow cytometry. 23 single cells clones were successfully established, from which four clones

were chosen in this study because they showed clear morphology differences (named as clone #1, #2, #3, and #4, Figure 1A). Clone #1 cells were elongated, clones #2 cells were spindle-like shaped, Clone #3 cells were cuboidal, whereas Clone #4 cells were rounded and looked much smaller than cells from the other three clones (Figure 1A). We then analyzed three cell morphometric parameters (cell area, circularity, and aspect ratio in Figure 1B) of these four MiaPaCa-2 clones by ImageJ. Indeed, cell area and aspect ratio of clone #4 were significantly smaller than the other three clones, whereas its circularity was significantly bigger (Figure 1B). These results demonstrated morphological heterogeneity of MiaPaCa-2 clones.

Differential proliferation and migration rate of MiaPaCa-2 clones

We then studied whether the MiaPaCa-2 clones show differences in their ability of proliferation and migration. First, we seeded the same number of cells from the four MiaPaCa-2 clones at day 0, cultured them for four days and imaged them every day from day 1 to day 4. Cell numbers were counted each day for each of the MiaPaCa-2 clones. We found that the clone #1 is the fastest-proliferation cell line, while the clone #3 is the slowest (Figure 2B). When compared with clone #4, all the other three clones displayed significant proliferation difference at day 4. The result suggests differential proliferation rate between the MiaPaCa-2 clones.

To investigate whether the MiaPaCa-2 clones have distinct migration rate, we employed the scratch wound healing assay (*13, 14*). Since cell proliferation contributes to wound closure in the scratch wound healing assay, to solely study cell migration in this assay we blocked cell proliferation during the process of the assay by administration of the DNA synthesis inhibitor thymidine (*15, 16*) in the cell culture medium 24 hours before inducing *in vitro* scratch. Results indicated that wound closure was significantly fast in clone #1 and clone #2 after 48-hour culture, relative to clone #3 and clone #4 (Figure 4C and 4D).

Genomic heterogeneity in the MiaPaCa-2 clones

We have demonstrated phenotypic heterogeneity in these four MiaPaCa-2 clones. We reasoned this phenotypic heterogeneity must come from genomic heterogeneity the MiaPaCa-2 clones, we therefore first analyzed their chromosome copy number profiles. Genomic DNA of these four MiaPaCa-2 clones was subjected to single-nucleotide polymorphism microarray (SNPa), and an in-house algorithm was used to derive their copy number profiles at 1 Mb resolution (Figure 3A). We previously benchmarked this method and demonstrated that SNPa produced similar results as the comparative genome hybridization array (*17*), which is the gold standard for chromosome copy number profile measurements (*18*). Chromosome copy number alterations were observed across the genome of the MiaPaCa-2 clones (Figure 3A). We then investigated the copy number variations (CNVs) between the MiaPaCa-2 clones. CNVs were derived by dividing the copy number of each clone by the median copy number. CNVs that are unique to a clone were observed in chromosomes 1, 2, 5, 7, 10, 11, 12, 14, 16, 22, and X. Results from SNPa and CNVs analysis suggest genomic heterogeneity in the MiaPaCa-2 clones.

Differential gene expressions between the MiaPaCa-2 clones.

We next investigated whether the MiaPaCa-2 clones showed heterogeneity at the transcriptional level. Toward this goal, we performed differential expression analysis for the four MiaPaCa-2 clones. We then compiled all the differential expressed genes associated with the clones and visualized them in a heatmap (Figure 4A). To generate this heatmap, the normalized read counts of each clone were divided by the median count of each gene to derive the differentially regulated genes between the clones. The heatmap contained the normalized read counts of genes that are uniquely regulated within a clone, with a threshold of $-1 < \log2(FC) < 1$. Hierarchical clustering of the genes revealed the group of genes that are uniquely regulated within a given clone (Figure 4A). K means clustering on the genes revealed 7 major clusters (Figure 4A). This result indicated differential gene expressions in the MiaPaCa-2 clones.

ITGAV is necessary and efficient for morphology change of MiaPaCa-2 clones

Integrin genes have been known to play an important role in focal adhesion formation, thus they are relevant to cell adhesion, spreading, migration, and cell shape change (*19, 20*). To investigate whether integrin genes are involved in morphological heterogeneity of the MiaPaCa-2 clones, we looked into the genes in the clusters of the heatmap (Figure 4A). Interestingly, we found that *ITGAV* is differentially expressed in cluster #5 among the MiaPaCa-2 clones. Specifically, ITGAV is significantly downregulated in clone #4 compared to other three clones (Figure 5A). Consistent with the deceased expression of *ITGAV* in clone #4, Western blotting showed that the ITGAV protein level was also significantly lower in clone #4 than in other three clones (Figure 4B and 4C). This decreased protein level may explain the rounded shape of clone #4 cells and their loose attachment to the cell culture plate (Figure 1A and data not shown).

To study whether ITGAV is sufficient to induce morphology change in the MiaPaCa-2 clones, an ITGAV protein fused with the fluorescent protein mApple (addgene plasmid #54866 by Michael Davidson lab) was transiently expressed in clone #4 (Figure 4C). As expected, expression of *ITGAV* induced morphology change of clone #4 cells from rounded to elongated (Figure 4D and 4E). Further quantification indicated the significant morphology differences between clone #4 with and without expression of *ITGAV* in it (Figure 5F). This result demonstrated that ITGAV is required for the spreading morphology of MiaPaCa-2 cells. We then investigated whether depletion of *ITGAV* would induce rounded shape of MiaPaCa-2 cells. We chose clone #1 cells because they are more elongated than clone #2 and #3 cells. Indeed, knockout of *ITGAV* caused most of clone #1 cells rounded up (Figure 5G and 5H). Quantification of cell morphometric parameters demonstrated the significant morphology changes of clone #1 upon loss of *ITGAV* (Figure 5K). Further Western blotting confirmed that the ITGAV protein level was significantly decreased in clone #1 when its ITGAV was depleted

(Figure 5I and 5J). Taken together, these results demonstrated that ITGAV is necessary and sufficient to induce morphology changes in the MiaPaCa-2 clones.

Discussion

One of the deadliest features of PDAC is its early systemic dissemination and tumor progression. Because of a high degree of intra- and inter-tumoral heterogeneity, the inability to diagnose PDAC at an early developmental stage has led to poor prognosis, as well as the obstacle to effective treatment. Thus, it is highly desirable to explore the tumoral heterogeneity and the underlying mechanism that are pivotal for PDAC prognostic improvement. In this study, we established four independent MiaPaCa-2 clones by using single-cell flow sorting that show clear distinct morphology (Figure 1A). This is consistent with previous reports showing that sub-populations of MiaPaCa-2 cells displayed differences in morphology (*21, 22*). This morphological heterogeneity may correlate with their functional differences as they show different proliferation and migration rate. Further genome-wide sequencing and transcriptional analysis on these four MiaPaCa-2 clones revealed their heterogeneity at the genomic and transcriptional levels. Very importantly, we identified an integrin gene ITGAV from our transcriptional analysis as a critical regulator of morphology change in the MiaPaCa-2 cells. In summary, our study systematically investigated the heterogeneity of PDAC cells at the phenotypic, genomic, and transcriptional levels and found how the genomic and transcriptional heterogeneity impacts phenotypic heterogeneity in MiaPaCa-2 PDAC cells.

With the development of genome-wide DNA sequencing and transcriptomic RNA-seq technologies, genomic and transcriptomic heterogeneity of the PDAC tumor has been well characterized over past decade (*3-10*), while some studies investigate the phenotypic heterogeneity in pancreatic cancer cells (*21-23*). However, no studies have been focused on how genomic and transcriptional heterogeneity drives phenotypic heterogeneity in pancreatic cancer cells according to our knowledge. The central dogma of molecular biology is key to

understanding the flow of information from genotype to phenotype. Here, however, we first investigated the phenotypic variations by establishing MiaPaCa-2 independent clones (Figure 1 and 2). By genomic sequencing and transcriptomic sequencing of the MiaPaCa-2 clones with different features, we identified their heterogeneity at the genomic and transcriptomic levels (Figure 3 and 4). In reverse, we identified ITGAV from the RNA-seq analysis that mediates the flow of information from transcriptomic heterogeneity to phenotypic heterogeneity (Figure 5). The integrin family of cell adhesion receptors has been implicated in many aspects of tumor development including tumor cell proliferation, migration, metastasis and survival (*20, 24*). In pancreatic cancer, some studies have shown that certain integrin family proteins are involved in pancreatic tumor growth, migration and invasion (*25-28*). In conclusion, our present study confirmed the multiple-level heterogeneity in MiaPaCa-2 cells and provided a mechanistic explanation how genomic variations drive phenotypic heterogeneity in pancreatic cancer cells.

Materials and Methods

Cell lines and tissue culture

The human pancreatic cell line MiaPaCa-2 was obtained from ATCC (www.atcc.org). Cells were maintained in a humidified atmosphere containing 5% CO_2 at 37°C in Dulbecco's modified Eagles medium (DMEM) supplemented with 10% fetal bovine serum (Genesee Scientific) and 1% Penicillin-Streptomycin (Sigma-Aldrich).

Generation of MiaPaCa2 clones by single-cell sorting

Four MiaPaCa-2 clones were generated by single-cell FACS sorting at Florida State University's Flow Cytometry Laboratory. Briefly, MiaPaCa-2 cell pellets were harvested after dissociated with Trypsin (Corning) at 37°C for 5 minutes. Cell pellets were washed once with PBS and resuspended with 1ml of PBS supplemented with 10% fetal bovine serum and 1% Penicillin-Streptomycin. Cell suspensions were filtered through a BD FACS tube with 70 μm strainer top.

Single cells were sorted using the FACSCanto instrument by forward scatter to a 96-well plate (Genesee Scientific). 23 MiaPaCa-2 single-cell clones were established after about 3-week culture under normal culture medium, of which 4 clones were expanded in 12-well plates and used in this study.

Scratch wound healing assay

Cell migration was evaluated by a scratch wound healing assay as previously described (*13, 14*). MiaPaCa-2 clone cells were seeded at a concentration of 4×10^5 cells/well (80% confluent) in 12-well plates and cultivated under normal culture medium until reaching fully confluent. Cells were then added with a final concentration of 2 mM thymidine to block cell proliferation for 24 hours. Next, each well was artificially wounded in the middle by creating a scratch with a plastic pipette 1000 µL tip on the cell monolayer. Each well was washed once with PBS to remove the floating cells and then cultivated under normal culture medium with 2 mM thymidine till the end of the assay. Images of scratch wounds were captured using EVOS microscope at 0, 24, and 48 hours after scratch wounding. The wound closure areas were measured with ImageJ after 24 and 48 hours. To avoid scratch area variation, “relative wound closure” area was calculated as [%] = (wound closure area^{T0} - wound closure area^{T48}) * 100 [%]/wound closure area^{T0}. Experiments were repeated at least three times.

Western blotting

Western blotting was performed using standard methods (*5*). Briefly, cell pellets were harvested and resuspended in RIPA buffer with addition of protein inhibitor cocktail as 50 µL buffer per million cells. Cell suspensions were then sonicated for 15 seconds and immediately put on ice for 30 minutes and cleared by centrifugation. 10-15 µL of protein lysis were run per lane of 4-12% Bis-Tris gels (Thermo Fisher Scientific) using MOPS buffer. Proteins were transferred to nitrocellulose membrane at 20V for 7 minutes using the iBlot™ 2 Transfer Stack (Thermo Fisher

Scientific). Membranes were blocked in 5% non-fat milk powder in TBS+0.1% Tween (TBST) and incubated overnight at 4°C in primary antibody diluted in TBS solution. Primary antibodies used are rabbit monoclonal antibody against ITGAV (ab179475, Abcam) and mouse monoclonal antibody against β-Actin (sc-47778, Santa Cruz Biotechnology). Membranes were incubated with corresponding horseradish peroxidase-conjugated second antibodies at room temperature for one hour. After three washes in TBST, membranes were exposed to ChromoSensor™ One-Solution (L00222V500, GenScript) for 3-5 minutes. Membranes were quickly washed three time and imaged

Single nucleotide polymorphism microarray

DNA isolation was performed using the Blood and Cell Culture DNA Mini Kit (QIAGEN). The isolated DNA samples were sent to the Center for Applied Genomics at the Children's Hospital of Philadelphia for the SNP array analysis using the Infinium Global Screening Array-24 v3.0 Kit (Illumina). The chromosome copy number analysis was performed as described previously. Heatmaps were plotted in R by using the algorithm gtrellis v.1.28.0 (*29*).

RNA-seq sample preparation and analysis

RNA isolation from the MiaPaCa-2 clones was performed by using the RNeasy Plus Micro Kit (QIAGEN). Libraries for RNA-seq were made with the NEBNext Ultra II Directional RNA Library Prep Kit for Illumina (NEB) per the manufacturer's instructions, followed by 150-bp paired-end sequencing with the Novaseq 6000 at Florida State University's Translational Science Laboratory, resulting in ~25,000,000 reads for each sample. Reads per kilobase million for each gene were calculated by normalization of the read of each gene by the sample's total read count (in millions) and by the gene length (in kilobases). The gene expression profile was plotted in R by using the algorithm gtrellis v.1.28.0 (*29*).

Acknowledgment

The authors would like to thank Drs. Cynthia Vied and Yanming Yang at Florida State University's Translational Science Laboratory for running the RNA-seq libraries and Dr. Beth Alexander at Florida State University's Flow Cytometry Laboratory for helping isolate the MiaPaCa-2 clones. We are grateful for the great service from the team at Florida State University's Biology Core Facilities. The authors thank all the lab members in Dr. Jerome Irianto's and Dr. Yue Julia Wang's laboratories for their valuable suggestions and assistance. The authors in this study were supported by startup funds from Florida State University, an award from the Florida Department of Health's Bankhead-Coley Cancer Research Program (award number 21B11), and a collaborative Trans-Network Project linked to the Physical Science-Oncology Project 5U01 CA214282 from the National Cancer Institute of the National Institutes of Health.

References

1. W. Park, A. Chawla, E. M. O'Reilly, Pancreatic Cancer: A Review. *JAMA* **326**, 851-862 (2021).
2. A. Adamska, A. Domenichini, M. Falasca, Pancreatic Ductal Adenocarcinoma: Current and Evolving Therapies. *Int J Mol Sci* **18**, (2017).
3. P. J. Campbell *et al.*, The patterns and dynamics of genomic instability in metastatic pancreatic cancer. *Nature* **467**, 1109-1113 (2010).
4. R. Maddipati, B. Z. Stanger, Pancreatic Cancer Metastases Harbor Evidence of Polyclonality. *Cancer Discov* **5**, 1086-1097 (2015).
5. S. M. Harding *et al.*, Mitotic progression following DNA damage enables pattern recognition within micronuclei. *Nature* **548**, 466-470 (2017).
6. A. P. Makohon-Moore *et al.*, Limited heterogeneity of known driver gene mutations among the metastases of individual patients with pancreatic cancer. *Nat Genet* **49**, 358-366 (2017).

7. J. Cros, J. Raffenne, A. Couvelard, N. Pote, Tumor Heterogeneity in Pancreatic Adenocarcinoma. *Pathobiology* **85**, 64-71 (2018).

8. J. Peng *et al.*, Single-cell RNA-seq highlights intra-tumoral heterogeneity and malignant progression in pancreatic ductal adenocarcinoma. *Cell Res* **29**, 725-738 (2019).

9. T. Y. Le Large *et al.*, Microdissected pancreatic cancer proteomes reveal tumor heterogeneity and therapeutic targets. *JCI Insight* **5**, (2020).

10. T. G. Krieger *et al.*, Single-cell analysis of patient-derived PDAC organoids reveals cell state heterogeneity and a conserved developmental hierarchy. *Nat Commun* **12**, 5826 (2021).

11. M. Wu, G. K. Arimura, A. A. Yunis, Purification and characterization of a plasminogen activator secreted by cultured human pancreatic carcinoma cells. *Biochemistry* **16**, 1908-1913 (1977).

12. R. Gradiz, H. C. Silva, L. Carvalho, M. F. Botelho, A. Mota-Pinto, MIA PaCa-2 and PANC-1 - pancreas ductal adenocarcinoma cell lines with neuroendocrine differentiation and somatostatin receptors. *Sci Rep* **6**, 21648 (2016).

13. L. G. Rodriguez, J. L. Guan, 14-3-3 regulation of cell spreading and migration requires a functional amphipathic groove. *J Cell Physiol* **202**, 285-294 (2005).

14. A. Grada, M. Otero-Vinas, F. Prieto-Castrillo, Z. Obagi, V. Falanga, Research Techniques Made Simple: Analysis of Collective Cell Migration Using the Wound Healing Assay. *J Invest Dermatol* **137**, e11-e16 (2017).

15. G. Chen, X. Deng, Cell Synchronization by Double Thymidine Block. *Bio Protoc* **8**, (2018).

16. J. B. Schvartzman, D. B. Krimer, J. Van't Hof, The effects of different thymidine concentrations on DNA replication in pea-root cells synchronized by a protracted 5-fluorodeoxyuridine treatment. *Exp Cell Res* **150**, 379-389 (1984).

17. J. Irianto *et al.*, DNA Damage Follows Repair Factor Depletion and Portends Genome Variation in Cancer Cells after Pore Migration. *Curr Biol* **27**, 210-223 (2017).

18. N. P. Carter, Methods and strategies for analyzing copy number variation using DNA microarrays. *Nat Genet* **39**, S16-21 (2007).

19. J. Z. Kechagia, J. Ivaska, P. Roca-Cusachs, Integrins as biomechanical sensors of the microenvironment. *Nat Rev Mol Cell Biol* **20**, 457-473 (2019).

20. J. S. Desgrosellier, D. A. Cheresh, Integrins in cancer: biological implications and therapeutic opportunities. *Nat Rev Cancer* **10**, 9-22 (2010).

21. N. Walsh, M. Clynes, J. Crown, N. O'Donovan, Alterations in integrin expression modulates invasion of pancreatic cancer cells. *J Exp Clin Cancer Res* **28**, 140 (2009).

22. N. Walsh *et al.*, Identification of pancreatic cancer invasion-related proteins by proteomic analysis. *Proteome Sci* **7**, 3 (2009).

23. Y. Iwagami *et al.*, miR-320c regulates gemcitabine-resistance in pancreatic cancer via SMARCC1. *Br J Cancer* **109**, 502-511 (2013).

24. S. E. Winograd-Katz, R. Fassler, B. Geiger, K. R. Legate, The integrin adhesome: from genes and proteins to human disease. *Nat Rev Mol Cell Biol* **15**, 273-288 (2014).

25. J. Schnittert *et al.*, Integrin alpha11 in pancreatic stellate cells regulates tumor stroma interaction in pancreatic cancer. *FASEB J* **33**, 6609-6621 (2019).

26. M. S. Mia, Y. Jarajapu, R. Rao, S. Mathew, Integrin beta1 Promotes Pancreatic Tumor Growth by Upregulating Kindlin-2 and TGF-beta Receptor-2. *Int J Mol Sci* **22**, (2021).

27. M. Kemper *et al.*, Integrin alpha-V is an important driver in pancreatic adenocarcinoma progression. *J Exp Clin Cancer Res* **40**, 214 (2021).

28. J. J. Grzesiak, K. C. Smith, D. W. Burton, L. J. Deftos, M. Bouvet, Integrin-mediated laminin-1 adhesion upregulates CXCR4 and IL-8 expression in pancreatic cancer cells. *Surgery* **141**, 804-814 (2007).

29. Z. Gu, R. Eils, M. Schlesner, gtrellis: an R/Bioconductor package for making genome-level Trellis graphics. *BMC Bioinformatics* **17**, 169 (2016).

Figure 1. Morphological heterogeneity of MiaPaCa-2 clones

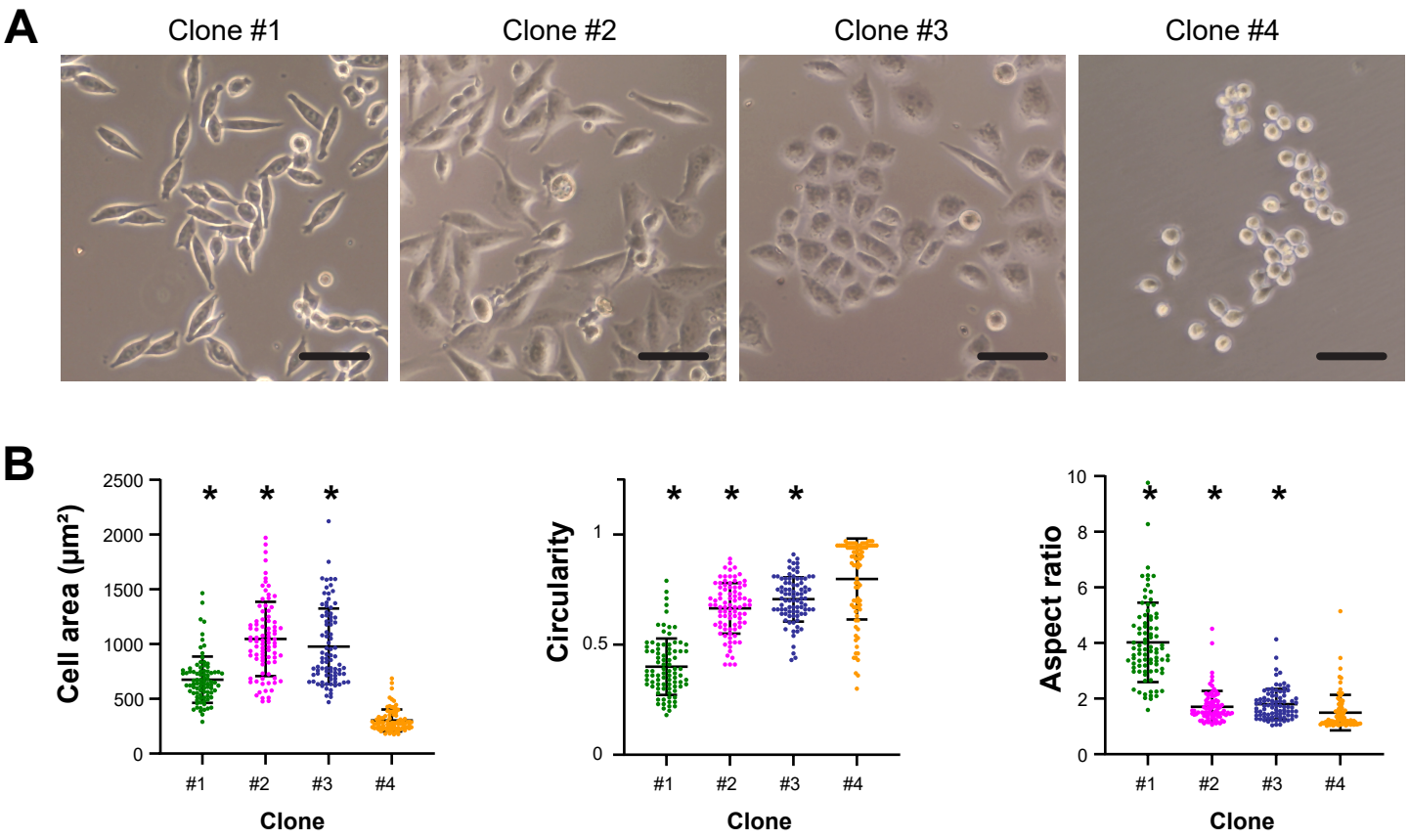

Figure 1. Morphological heterogeneity of MiaPaCa-2 clones. (**A**) Representative images of four MiaPaCa-2 clones isolated and expanded from single-cell flow sorting, showing their morphological differences (scale bar = 50 μm). (**B**) Three cell morphometric parameters (cell area, circularity, and aspect ratio) analyzed by imageJ, showing significant differences between the MiaPaCa-2 clones. Significant analysis of clones #1, #2, and #3 vs clone #4 (Welch's t test, p value < 0.05).

Figure 2. Differential proliferation and migration rate of MiaPaCa-2 clones

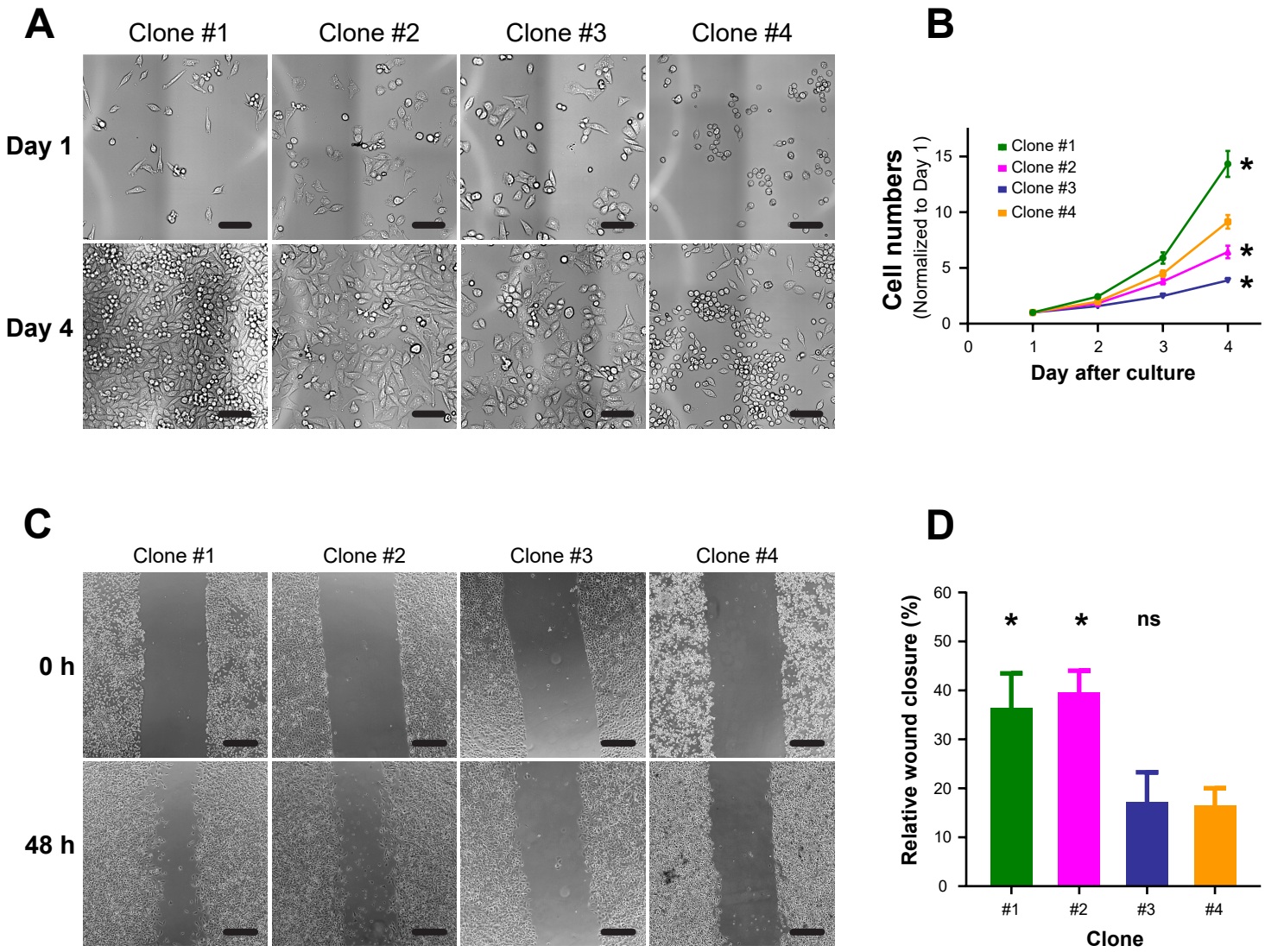

Figure 2. Differential proliferation and migration rate of MiaPaCa-2 clones. (**A**) Representative images of the MiaPaCa-2 clone cells on day 1 and day 4 after seeding (scale bar = 100 μm). (**B**) Plot of cell number increases of different MiaPaCa-2 clones over a period of 4-day culture. Cell number increases were normalized to the cell number of day 1 in each of the clones. (**C**) Representative images of the four MiaPaCa-2 clones on zero hour and 48 hours after *in vitro* scratch (scale bar = 300 μm). (**D**) Plot of relative wound closure of different MiaPaCa-2 clones at 48-hour time point. Significant analysis of clones #1, #2, and #3 vs clone #4 vs clones #4 (Welch's t test, p value < 0.05).

Figure 3. Genomic heterogeneity between the MiaPaCa-2 clones

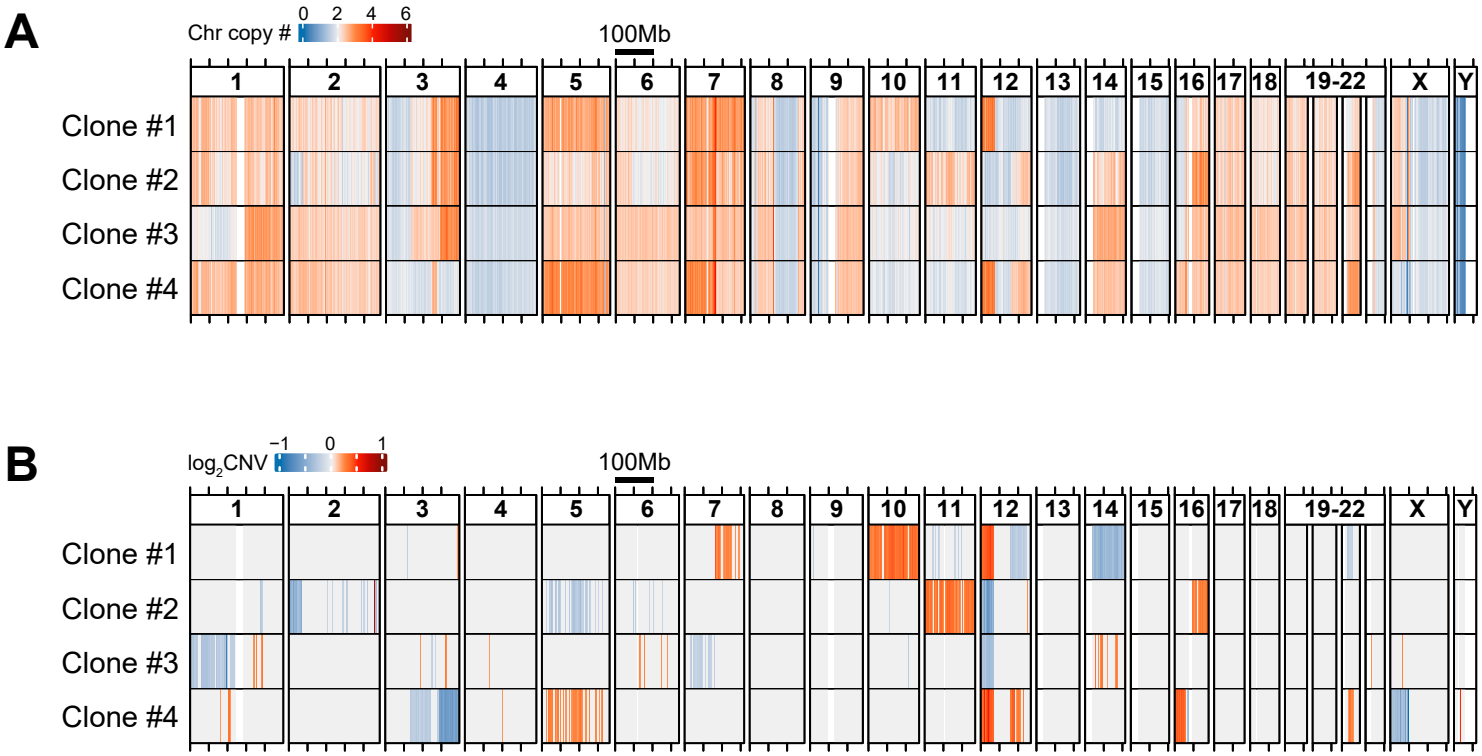

Figure 3. Genomic heterogeneity between the MiaPaCa-2 clones. (**A**) Genomic DNA of the MiaPaCa-2 clones was subjected to SNPa and the resulting data was used to derive chromosome copy numbers of the clones within 1Mb binning windows. The heatmaps illustrate chromosome copy numbers across the whole genome, where blue indicates chromosome loss (<2) and red indicates chromosome gain (>2). (**B**) The copy number variations (CNVs) between the clones were derived by dividing the copy number of each clone by the median copy number. CNVs that are unique to a clone were observed in chromosomes 1, 2, 5, 7, 10, 11, 12, 14, 16, 22, and X, suggesting genomic heterogeneity between the clones.

Figure 4. Differential gene expressions between the MiaPaCa-2 clones

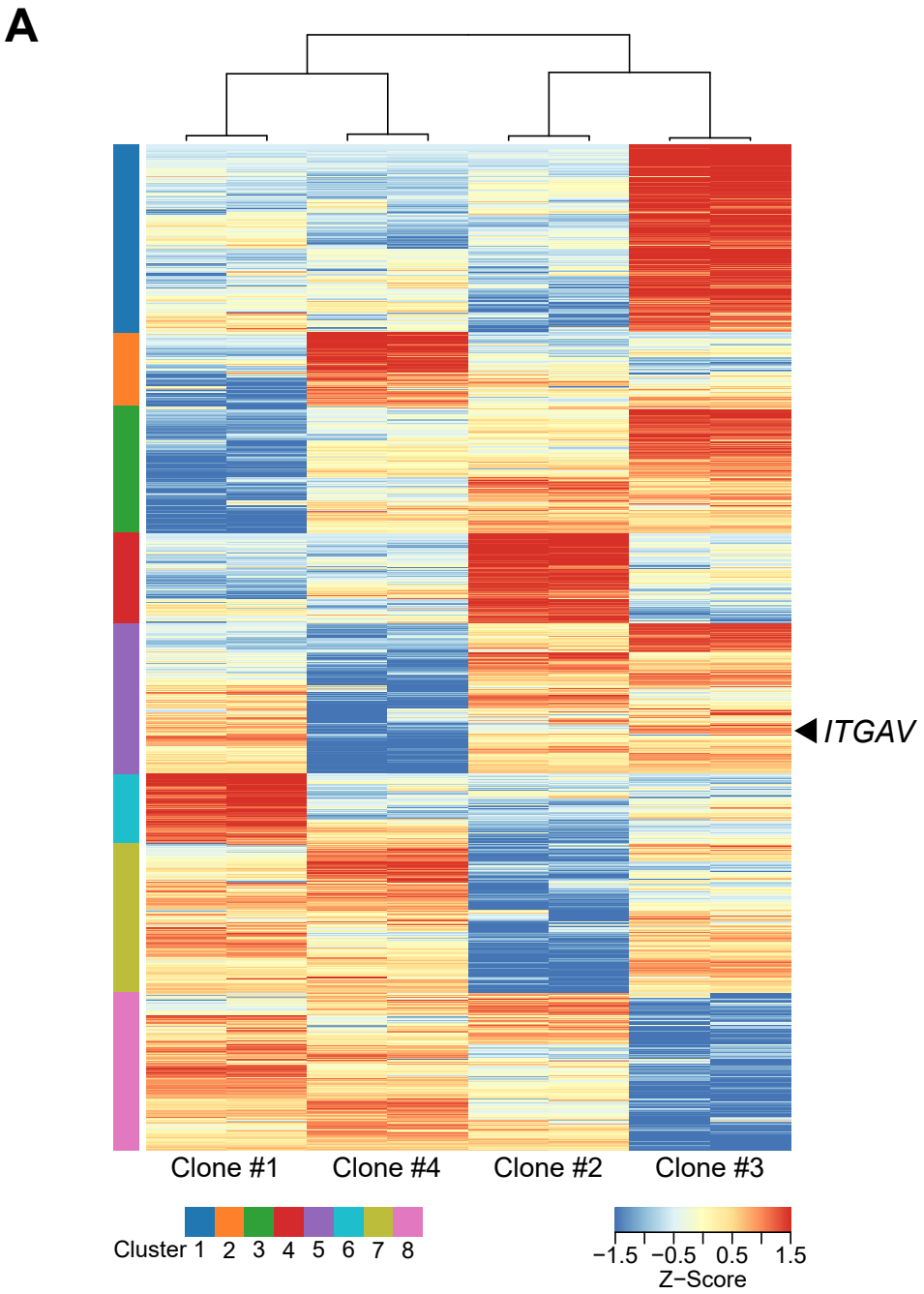

Figure 4. Differential gene expressions between the MiaPaCa-2 clones. (**A**) The MiaPaCa-2 clones were subjected to RNA-seq. The normalized read counts of each clone were divided by the median count of each gene to derive the differentially regulated genes between the clones. The heatmap contains the normalized read counts of genes that are uniquely regulated within a clone, with a threshold of $-1 < \log2(FC) < 1$. Hierarchical clustering of the genes reveals the group of genes that are uniquely regulated within a given clone.

Figure 5. ITGAV is necessary and sufficient for morphology change of MiaPaCa-2 clones

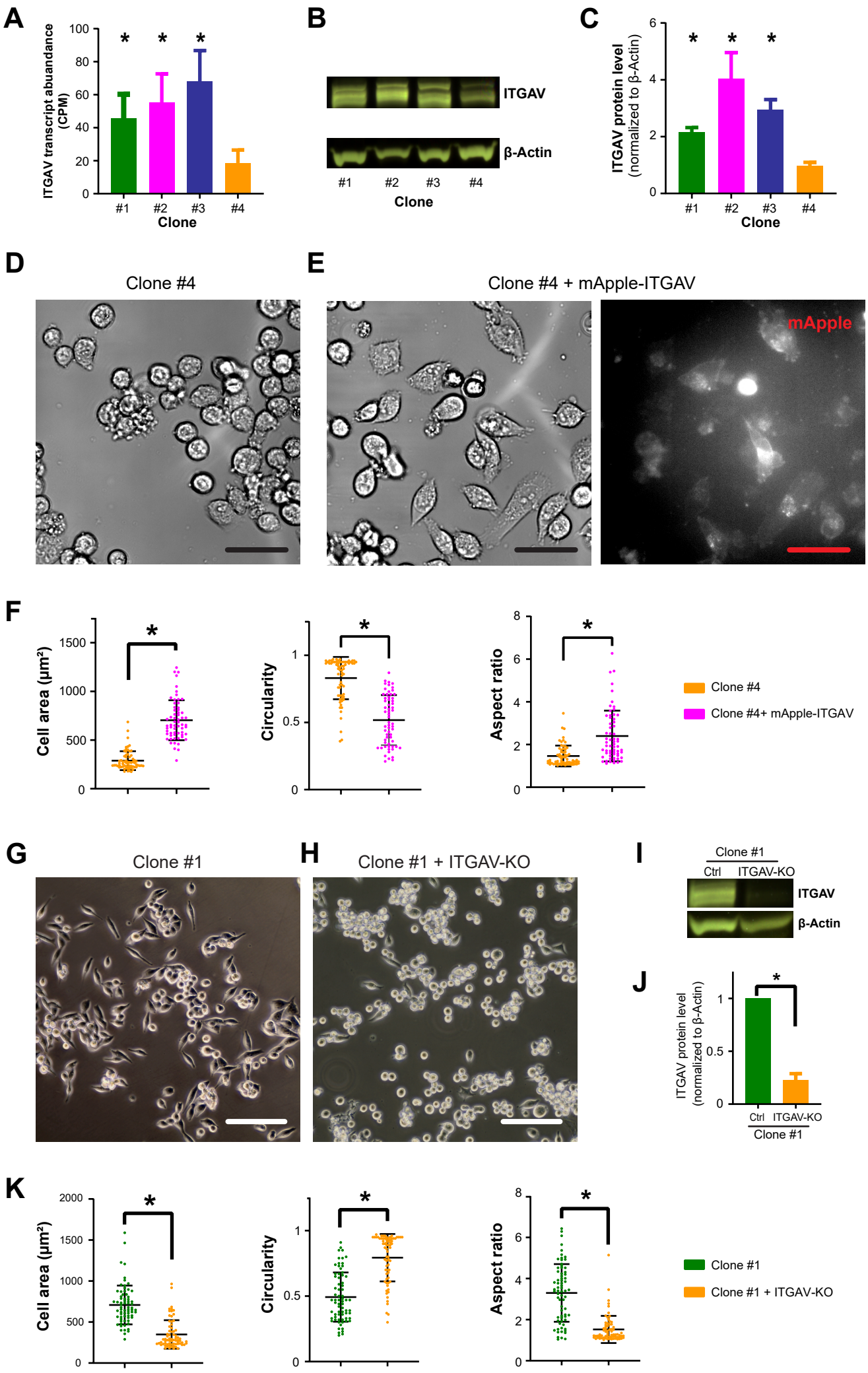

Figure 5. ITGAV is necessary and sufficient for morphology change of MiaPaCa-2 clones. (**A**) *ITGAV* transcript quantification in RNA-seq of the MiaPaCa-2 clones (normalized to counts per million reads, CPM), showing clone #4 has significantly decreased expression of *ITGAV* (Welch's t test, p value < 0.05). (**B**) Western blot of the ITGAV protein in the MiaPaCa-2 clones (upper band) and the β-Actin protein as the loading control (lower band). (**C**) Quantification of the ITGAV protein from **B**, normalized to β-Actin, showing clone #4 has significant lower level of the ITGAV protein (Welch's t test, p value < 0.05). (**D** and **E**) Representative images of the MiaPaCa-2 clone #4 (**D**) and clone #4 transiently transfected with mApple-ITGAV (**E**), showing that clone #4 cells are elongated when transfected with ITGAV (mApple positive) (scale bar = 50 μm). (**F**) Three cell morphometric parameters (cell area, circularity, and aspect ratio) analyzed by imageJ, showing significant differences between clone #4 and clone #4 expressing mApple-ITGAV (Welch's t test, p value < 0.05). (**G** and **H**) Representative images of the MiaPaCa-2 clone #1 (**G**) and clone #1 transduced with a CRISPR vector targeting ITGAV (**H**), showing majority of cells of clone #1 upon depletion of *ITGAV* changed from elongated to rounded (scale bar = 100 μm). (**I** and **J**) Western blot showing clone #1 upon knockout of *ITGAV* significantly reduced the ITGAV protein (**I**), which was quantified in **J** (normalized to β-Actin, Welch's t test, p value < 0.05). (**K**) Three cell morphometric parameters (cell area, circularity, and aspect ratio) analyzed by imageJ, showing significant differences between clone #1 and clone #1 with the depletion of *ITGAV*.